

Rational designing of double-sided nail plate joints using the finite element method

Tinozivashe Zhou[†]

School of the Environment, University of Brighton, Moulsecoomb, Lewes Road, Brighton, East Sussex, BN2 4GJ, United Kingdom

Z. W. Guan[‡]

Department of Engineering, The University of Liverpool, Brownlow Hill, Liverpool, L69 3GQ, United Kingdom

(Received May 8, 2006, Accepted September 20, 2007)

Abstract. Double-sided punched metal plate timber fasteners present projections on both sides, which offer improved joint fire resistance and better joint aesthetics. In this paper, 3-D nonlinear finite element models were developed to simulate double-sided nail plate fastener timber joints. The models, incorporating orthotropic elasticity, Hill's yield criterion and elasto-plasticity and contact algorithms, are capable of simulating complex contact between the tooth and the timber and between the base plate and the timber in a fastener. Using validated models, parametric studies of the double-sided nail plate joints was undertaken to cover the tooth length and the tooth width. Optimal configuration was assumed to have been attained when increase in nail plate tooth width did not result in a raise in joint capacity, in conjunction with the optimum tooth length. This paper presents the first attempt to model and optimise tooth profile of double-sided nail plate fastener timber joints, which offers rational designs of such fasteners.

Keywords: contact; double-sided nail plate fastener; finite element; parametric study; rational design.

1. Introduction

Timber used in construction is usually available in limited lengths due to constraints imposed by production and transportation processes. In order for timber to be utilised in construction, it requires jointing to produce the lengths, forms and shapes necessary for fabricating the designed structural systems. One of the modern timber connection methods is punched metal plate fasteners, also commonly referred to as nail plates.

Such fasteners can either be single-sided or double-sided. The former, with projections on one side, were invented and patented in the United States of America in 1952 by Carroll Sanford (Wolfe *et al.* 1996). At that time, as is mostly the case at the present moment, they were primarily intended

[†] Ph.D., Lecturer, E-mail: tinozhou@ntlworld.com

[‡] Ph.D., Senior Lecturer, Corresponding author, E-mail: zguan@liverpool.ac.uk

for roof and floor truss joint fabrication.

Research on theoretical analysis of the single-sided punched metal plate timber fasteners is limited to the applications in truss connections (Foschi 1977, Foschi 1979, Cramer 1990). Optimisation in relation to the single-sided punched metal plate fasteners is also linked to the truss connections (Šilih *et al.* 2005). There is hardly any research on optimisation of nail profiles of the punched metal plate timber fasteners, especially for the double-sided metal plate fasteners.

Double-sided punched metal plate timber fasteners present projections on both sides. Such connectors offer two distinct potential advantages over their single-sided counterparts (Malinowski 1985). These are:

- (1) improved joint fire resistance since the metal connectors are sandwiched between the timber members connected, and
- (2) better joint aesthetics since the metal connectors are concealed by the timber members connected.

Fig. 1 shows a typical double-sided punched metal plate fastener. Identified potential fields of application for the double-sided nail plates were given as multiple ply timber trusses, compound columns and moment resisting frame corner joints, all of which could be prefabricated (Malinowski 1985). In continuous strip form, the nail plates were also identified as potentially useful for fabrication of compound beams for large span roof and floor construction. A central feature of all the joints proposed (Malinowski 1985) was that the symmetry of the connection was maintained, even if it meant using wooden packing and outer straps to achieve joint symmetry.

The current research is focussed on developing a new approach for optimising the tooth profile of a double-sided punched metal plate fastener in softwood timber joints. The prototype double-sided nail plate used for this study was proposed and supplied by Wolf Systems (UK) Limited, a manufacturer of traditional nail plates. This particular type of nail plate was based on the geometry of an existing single-sided plate, as shown in Fig. 2.

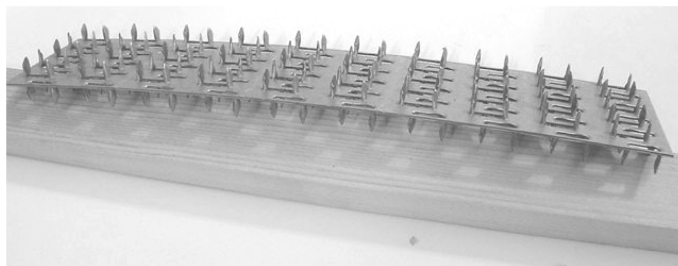


Fig. 1 Typical double-sided punched metal plate fastener (or nail plate)

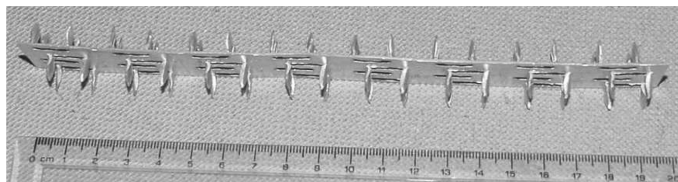


Fig. 2 Proprietary prototype double-sided punched metal fastener produced by Wolf Systems UK (the Wolf plate)

Tooth/plate profiles, interaction between the tooth and the timber and anisotropic material properties of the timber introduce complexities of double-sided punched metal plate fastener joints. Therefore, the most promising way to study the fastener is to develop 3-D nonlinear finite element (FE) models with appropriate contact algorithms. Using validated FE models, optimising of the fastener can be undertaken by varying tooth/plate profiles and the properties of the constituent materials.

In general, modelling of problems involving bodies coming into contact and interacting is complex and requires significant time investment in model development. For single-sided nail plate joints, the problem is further complicated by the fact that the two bodies coming into contact, the timber and the steel tooth, are both deformable (Adjanohoun *et al.* 1999). Modelling of double-sided nail plate joints is even more complex because of loading eccentricity on the connector. This results in complex motions in which the nail plate teeth have a tendency to penetrate more into the timber at some points whilst simultaneously withdrawing from other points as it responds to the eccentricity moments. The timber, for its own, has a tendency to move away from the nail plate teeth as they bend under load. All these motions are predominantly resisted by the friction between the wood and the nail plate teeth. Yet Adjanohoun *et al.* (1999) experiencing serious model convergence problems, could only manage to model the joint with coefficients of friction up to 0.2. The contact problem, therefore, predominantly dictated the choice of the model used for nail plate optimisation in this study.

In this paper, 3-D nonlinear finite element models were developed to simulate double-sided punched steel fasteners. In the models, timber in tension parallel to the grain was modelled using orthotropic elasticity and Hill's yield criterion, and elasto-perfect plasticity was used for the timber under compression (embedding). Contact algorithms, capable of modelling both small slide and finite slide, were used to simulate complex contact between the tooth and the timber, and between the base plate and the timber. Using validated models, parametric studies of the double-sided nail plate was undertaken to cover the tooth length and the tooth width. Optimal configuration was assumed to have been attained when increase in nail plate tooth width did not result in a raise in its capacity, in conjunction with the optimum tooth length. This paper presents the first attempt to model and optimise tooth profile of double-sided nail plate fastener timber joints, which offers rational designs of such fasteners.

2. Finite element formulation

Different constitutive models need to be applied to timber members and punched steel plates in the joint in order to obtain reasonable simulation of overall joint behaviour. Contact algorithms were also required in development of the numerical simulation.

2.1 Constitutive laws for orthotropic materials

Wood is an anisotropic material with different material properties in different directions (Bodig and Jayne 1982). For modelling purposes, and under appropriate conditions, wood may be assumed to be orthotropic (Pattorn-Mallory *et al.* 1997). If an orthotropic elasto-plastic material model is adopted, the elastic behaviour is defined in terms of the 9 independent engineering constants, three elasticity moduli, three shear moduli and three Poisson's ratios. The corresponding constitutive law

for the material is stated as (Hibbitt *et al.* 2002)

$$\{\varepsilon\} = [C]_{orth}\{\sigma\} \quad (1)$$

where $\{\varepsilon\}$ is strain tensor, $\{\sigma\}$ is stress tensor and $[C]_{orth}$ is orthotropic elastic compliance matrix, i.e.

$$\{\varepsilon\} = \{\varepsilon_L \ \varepsilon_R \ \varepsilon_T \ \gamma_{RT} \ \gamma_{LT} \ \gamma_{LR}\}^T = \{\varepsilon_{ij}\}^T = \{\varepsilon_{ji}\}^T \quad (i, j = 2, 3, 1) \quad (2)$$

$$\{\sigma\} = \{\sigma_L \ \sigma_R \ \sigma_T \ \tau_{RT} \ \tau_{LT} \ \tau_{LR}\}^T = \{\sigma_{ij}\}^T = \{\sigma_{ji}\}^T \quad (i, j = 2, 3, 1) \quad (3)$$

$$[C]_{orth} = \begin{bmatrix} \frac{1}{E_T} & -\frac{\nu_{LT}}{E_L} & -\frac{\nu_{RT}}{E_R} & 0 & 0 & 0 \\ -\frac{\nu_{TL}}{E_T} & \frac{1}{E_L} & -\frac{\nu_{RL}}{E_R} & 0 & 0 & 0 \\ -\frac{\nu_{TR}}{E_T} & -\frac{\nu_{LR}}{E_L} & \frac{1}{E_R} & 0 & 0 & 0 \\ 0 & 0 & 0 & \frac{1}{G_{TL}} & 0 & 0 \\ 0 & 0 & 0 & 0 & \frac{1}{G_{LR}} & 0 \\ 0 & 0 & 0 & 0 & 0 & \frac{1}{G_{RT}} \end{bmatrix} \quad (4)$$

The corresponding relations of two Cartesian co-ordinate systems, used in the numerical modelling and the conventional timber orientations, are 1(*T*) - tangential direction, 2(*L*) - longitudinal direction and 3(*R*) radial direction.

For a symmetric stiffness matrix (based on orthotropic material assumption), the following relationships have to hold true

$$E_i \nu_{ij} = E_j \nu_{ji} \quad (i, j = T, L, R) \quad (5)$$

Hill's potential function (Hill 1948) has been successfully utilised to simulate anisotropic yielding of timber (Zhu 2003, Zhu *et al.* 2005). The yield surface is assumed to be anisotropic and the potential function proposed by Hill, which is stated as

$$f(\sigma_{ij}) = \sqrt{F_{11}(\sigma_{22} - \sigma_{33})^2 + F_{22}(\sigma_{33} - \sigma_{11})^2 + F_{33}(\sigma_{11} - \sigma_{22})^2 + 2(N_{12}\sigma_{12}^2 + N_{23}\sigma_{23}^2 + N_{31}\sigma_{31}^2)} \quad (6)$$

where $F_{ii}(i = 1, 2, 3)$ and $N_{ij}(i \neq j = 1, 2, 3)$ are constants obtained by tests of the material in different orientations and are defined as follows

$$F_{ii} = \frac{(\sigma^0)^2}{2} \left(\frac{1}{\sigma_{jj}^2} + \frac{1}{\sigma_{kk}^2} - \frac{1}{\sigma_{ii}^2} \right) = \frac{1}{2} \left(\frac{1}{R_{jj}^2} + \frac{1}{R_{kk}^2} - \frac{1}{R_{ii}^2} \right) \begin{cases} i = 1, 2, 3 \\ j = 2, 3, 1 \\ k = 3, 2, 1 \end{cases} \quad (6a)$$

$$N_{ij} = \frac{3}{2} \left(\frac{\tau^0}{\bar{\sigma}_{ij}} \right)^2 = \frac{3}{2R_{ij}^2} \quad (i \neq j = 1, 2, 3) \quad (6b)$$

R_{ij} are yield ratios which relate the yield level for stress component σ_{ij} to the reference yield stress σ^0 of the material. The yield ratios are defined as follows

$$R_{ij} = \begin{cases} \frac{\bar{\sigma}_{ij}}{\sigma^0}, & \text{if } i = j \\ \frac{\bar{\sigma}_{ij}}{\tau^0}, & \text{if } i \neq j \end{cases} \quad (7)$$

$$\tau_0 = \frac{\sigma^0}{\sqrt{3}} \quad (7a)$$

For the orthotropic material plasticity, the associated flow rule used is given by

$$d\{\varepsilon\}_{pl} = d\lambda \left\{ \frac{\partial f}{\partial \{\sigma\}} \right\} = \frac{d\lambda}{f} \{b\} \quad (8)$$

where $d\lambda$ is a proportionality constant termed the plastic multiplier, and

$$\{b\} = \begin{bmatrix} -F_{22}(\sigma_{33} - \sigma_{11}) + F_{33}(\sigma_{11} - \sigma_{22}) \\ F_{11}(\sigma_{22} - \sigma_{33}) - F_{33}(\sigma_{11} - \sigma_{22}) \\ -F_{11}(\sigma_{22} - \sigma_{33}) + F_{22}(\sigma_{33} - \sigma_{11}) \\ 2N_{12}\sigma_{12} \\ 2N_{31}\sigma_{31} \\ 2N_{23}\sigma_{23} \end{bmatrix} \quad (9)$$

At a microscopic level, timber has a cellular structure that is made up of lumens and cell walls (Forest Products Laboratory 1999). Reiterer and Stanzl-Tschegg (2001) showed that due to this structure, timber cells buckle and collapse under compressive loads. In the longitudinal direction, they reported plastic softening (post-peak) in their specimens. Perpendicular to the grain they reported extended yielding plateaux followed by significant hardening after the cell walls had collapsed into the lumens and the wood densified. This type of hardening is only feasible in nail plate joints well after failure. Therefore, no material hardening is assumed for modelling the timber in the current research.

2.2 Constitutive relationships for metal plate fastener

After initial yielding, total deformation will be partly elastic and partly plastic. Therefore, for any increment of stress, the related strain increment $d\varepsilon_{ij}$ is composed of two parts,

$$\{d\varepsilon_{ij}\} = \{d\varepsilon_{ij}\}_{el} + \{d\varepsilon_{ij}\}_{pl} \quad (10)$$

The associated flow rule, which gives the relationship between the plastic strain increment and the stress increment is given by (Nayak and Zienkiewicz 1972, Chen and Han 1988, Drucker 1988)

$$\{d\varepsilon_{ij}\}_{pl} = d\lambda \left\{ \frac{\partial f}{\partial \sigma_{ij}} \right\} \quad (11)$$

where f is a yield function. Furthermore, the complete elasto-plastic incremental stress-strain relationship can be expressed as follows.

$$d\{\sigma\} = [D]_{ep} d\{\varepsilon\} \quad (12)$$

where $[D]_{ep}$ is the elasto-plastic matrix. The above algorithms have been successfully used in modelling of dowel type joints made with solid and hollow steel dowels (Guan and Rodd 2000, 2001, 2003).

2.3 Contact algorithm

Abaqus/Standard (Hibbitt *et al.* 2002) offers comprehensive contact algorithms, which allow an initially separated surface pair get into contact or initially contacted surfaces to be separated after applying loads. Those algorithms have been successfully used to simulate various contact cases in dowel type timber joints (Guan and Rodd 2000, 2001), shear plate joints (Guan and Rodd 2003), and prestressed glulam beams (Guan *et al.* 2005). Therefore, the same contact algorithms are adopted to model contact conditions in the double-sided nail plate timber fasteners.

The fabrication of timber joints by pressing in of nail plates brings the fastener surfaces around the embedded teeth into contact with the wood. This process sets up forces normal to the contacting surfaces. Under incremental lateral joint loading, these normal forces also increase in magnitude and there is a tendency for the surfaces in contact to slide relative to each other as the nail plates pull out of the wood. Due to the roughness of the surfaces in contact, the withdrawal of the nail plate teeth is resisted by frictional forces that are set up between the metal and wood surfaces. This interaction, tangential to the contact surfaces, manifests as shear stresses. The magnitude of sliding that occurs, however, is governed by the limiting resistive shear stresses given by

$$\tau_R = \mu p \quad (13)$$

where τ_R is limiting frictional shear stress, μ is coefficient of friction, and p is contact pressure acting normal to the contact surface.

Numerically, the contact problem is treated as a boundary condition problem whereby constraints are applied at the nodes on surfaces that come into contact, and are removed when surfaces formerly in contact are separated. In modelling of the nail plate fastener, the contact problem is defined by pairing of the surfaces that are likely to come into contact during simulation and specifying the type of interaction they will experience. In these contact pairs, one surface is defined as a master surface, which cannot be numerically penetrated by the nodes of the other surface (called the slave surface). For frictional contact problems, the interaction is simulated using the Coulomb friction model. This is an idealised model that is based on sticking-sliding behaviour of the interacting surfaces. The sliding of the surfaces is only implemented when the exerted frictional shear stresses exceed the limiting value given by Eq. (13).

However, there is considerable numerical difficulty in simulating ideal sliding behaviour in contact problems. Simplified models, therefore, are often employed. A penalty function is therefore

used, in which very small elastic sliding is permitted during the phase when the contact surfaces are sticking.

To simulate contact it is necessary to identify the areas within a contact pair actually in contact or out of contact, then to apply and remove constraints over these surface areas accordingly, and finally to calculate the magnitude of the contact pressures and shear stresses. In analysis, the simulation is implemented in two broad iteration phases, namely contact state iteration and equilibrium iteration. Both schemes of iteration are based on the numerical solution of the equilibrium equation. The process to establish the initial contact state and further to update the contact conditions through each iteration is described as the most challenging in contact analysis by Rahman *et al.* (1984). The criteria are based on the difference between the limiting frictional stress and the calculated shear stress on the slave node, which are applied to decide the sticking/sliding state of modes in contact.

In their algorithm, Rahman *et al.* (1984) used the forward interpolation to fix the sliding slave nodes to the master surface. The equilibrium iterations are then conducted using the latest fixed configuration from contact state iteration phase.

3. Validation of the FE modelling

The finite element models developed above needed to be validated against experimental results. Validations were taken for a single-tooth, two-tooth and eight-tooth joint models. Fig. 3 shows mesh generations for these models. Orthotropic elasto-perfect plastic material properties were used for timber modelling and elasto-plastic properties with strain hardening for nail plate modelling (Zhou 2005).

C3D8 linear brick elements were chosen for modelling the nail plate teeth because of their efficient performance in contact problems. However, the same elements experience shear locking in bending. The shear locking problem was overcome by mesh refinement, which resulted in the teeth having a finer mesh in the main sliding direction than the timber. The master surfaces were formed on the nail plate to prevent them from being numerically penetrated by the timber (slave surfaces). It is always recommended that the slave surfaces be more finely meshed than master surfaces to prevent solution divergence.

Definition of the exterior faces of the tooth and timber recess as a single contact surface respectively made numerical contact between them unstable. This was because the normals to the nodes along the 90° edges so formed were interpreted by the adopted contact algorithm as being oriented at angles other than right angles. The problem was overcome by defining each face as a surface and pairing corresponding surfaces on the timber and teeth in slave/master relationships. Each tooth interaction region, therefore, was defined by 10 contact surfaces, 5 on the tooth and 5 on the wood.

The basic units making up the prototype double-sided nail plates were 24 mm wide × 25 mm long modules with four teeth in two rows on either side. The tooth rows on each side were spaced at 11.5 mm centre-to-centre with an offset of 4 mm in the plate longitudinal direction. This basic configuration is illustrated in Fig. 3.

For a full double-sided joint made from laterally pressing loading, successive pairs of tooth rows on each side of the nail plate form force-couple systems, which cause each module to be deformed in a double curvature. Assuming an internal module for the modelling, the appropriate boundary

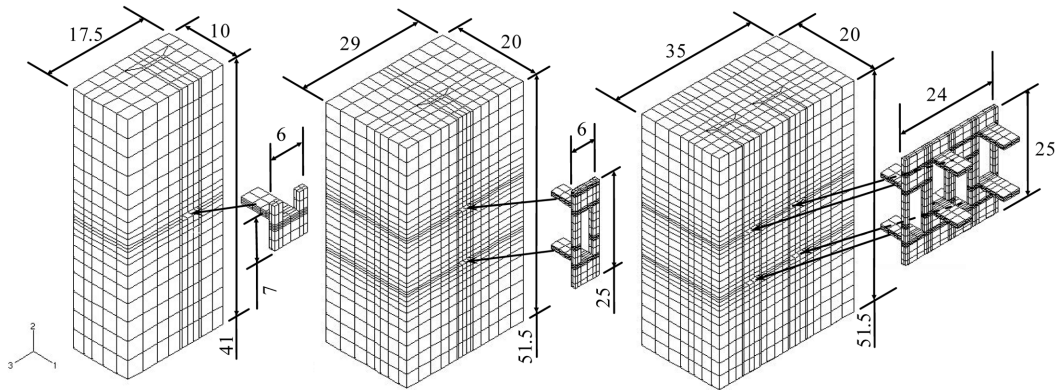


Fig. 3 Mesh generations for single-tooth, two-tooth and eight-tooth models

conditions were to constrain the module ends for translation in both horizontal directions (model 1- and 3-directions). The vertical direction (model 2-direction) remained unconstrained. Constraining the nail plate module in the model 1-direction prevented plate rigid body rotation, due to eccentricity moments, about the model 3-direction. In real joints, this rotation is prevented by frictional shear stresses generated between the teeth and the wood. Therefore, only the residual friction component, required to resist nail plate tooth withdrawal, was input into the model. Using the Coulomb model, the required friction was established iteratively, giving a value of $\mu = 0.24$.

4. Single-tooth model of load-slip behaviour

Effective wood material properties for the connected zone were inversely determined using the single-tooth joint model (Zhou 2005). The load-slip behaviour for the calibrated single-tooth joint FE model is shown Fig. 4. The experimentally determined bounding characteristics for tooth load capacity, and stiffness at the serviceability limit state and at the ultimate limit state are also shown together with a typical average experimental curve. The FE model curve showed good agreement with the experimental results. The model was therefore accepted for replication to build the double-sided punched metal plate fastened joint models.

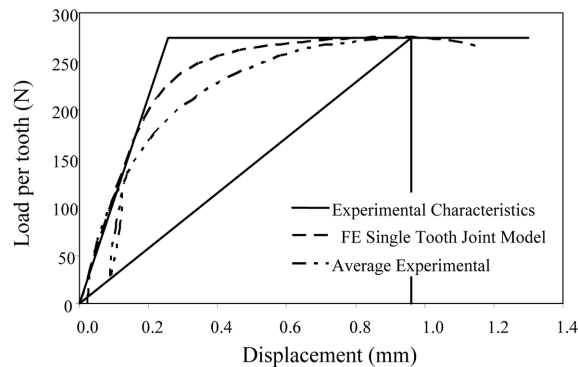


Fig. 4 Single-tooth joint load-slip curves for the calibrated FE model and comparable test specimens

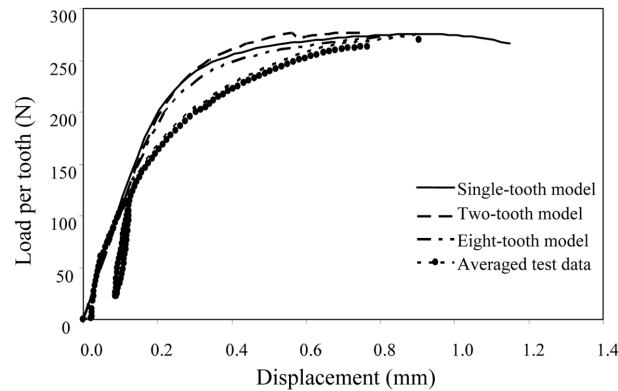


Fig. 5 Effect of model size

5. Multi-tooth model of load-slip behaviour

5.1 Effect of model size

The effect of tooth length was analysed using the two-tooth joint model and optimisation for tooth width was undertaken using the eight-tooth model. These models are only fractions of the full joint. To assess the effect of this simplification, the performance of these models is compared to experimental results.

Three joint models have been investigated; the single-tooth joint model, the two-tooth joint model and the eight-tooth joint model. For the same material properties, the effect of each of these models on the modelled load-slip behaviour is shown in Fig. 5. There is a good general agreement between the models, and reasonably good correlation between the model results and test results also exists. The eight-tooth model is slightly less stiff because of the eccentric loading applied to the base plate, an aspect not simulated in the other two models. It can be concluded, therefore, that the assumption of equal load distribution holds, at least in the sense of yielding, the same capacity per tooth from the three FE models.

5.2 Effect of load-shearing of teeth

The Wolf plate is doubly eccentric. The three FE models used so far have not directly taken into account the full effect of these eccentricities. Owing to the high iteration costs accruable from dealing with complex contact, attempts to model the full joint are not viable. To assess the effect of eccentric load shearing of the teeth, the full nail plate was modelled on its own, without wood, using concentrated loads applied to the teeth. Constraints were applied to prevent out-of-plate rotation of the base plate in line with the deformed shape shown in Fig. 6. Further restraints were also applied to prevent in-plane rotation of the base plate. These constraints are all idealised since they do not exist in practice, where more of the beam-on-elastic-foundation situation prevails. Tooth loads were applied so as to shear the plate parallel to its principal direction.

The moment-rotation behaviours of the teeth closest and furthest from the centre of rotation are compared in Fig. 7. The tooth furthest from the centre of rotation marginally undergoes less rotation

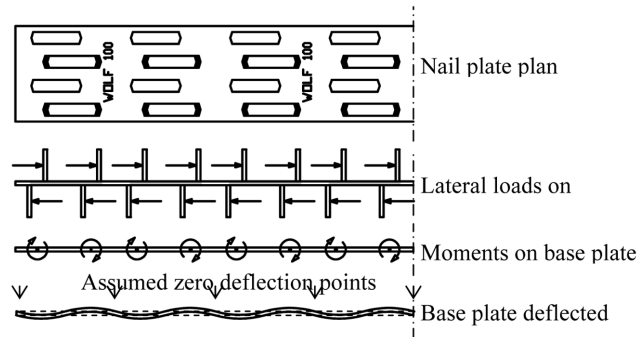


Fig. 6 Nail plate loads and assumed out-of-plane deflected shape of base plate

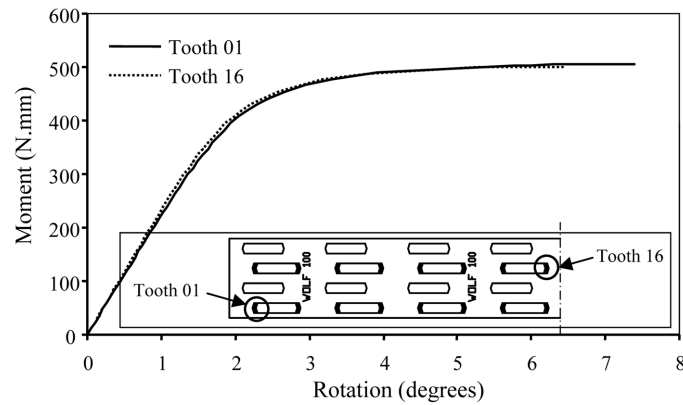


Fig. 7 Effect of eccentric load shearing of teeth

about the root for the same applied moment in the elastic state. This is due to the larger reactions, acting perpendicular to the plate principal direction, which resist the base plate in-plane rotation. This leads to a resultant force acting at an angle to the plate principal direction. The larger resultant force leads to early yielding of the furthest tooth but the curves crossover in the plastic range. However, load shearing effects from the model were detected as minimal. In practice the flexible constraints of teeth bearing on wood may produce a more pronounced effect.

5.3 Prediction of joint separation

The tooth-wood interface was modelled so as to allow the surfaces in contact to slide relative to each other, simulating tooth withdrawal, once the frictional resistance had been overcome. This process then models the tooth withdrawal process in real joints. The joints separation from the eight-tooth FE model are compared to the experimental results from three categories of tests conducted, namely in-direction, against-direction and full nail plate joint tests (Zhou 2005) in Fig. 8. Reasonably good model prediction is evident in all three cases. The model can, therefore, be accepted as having performed very well in this respect.

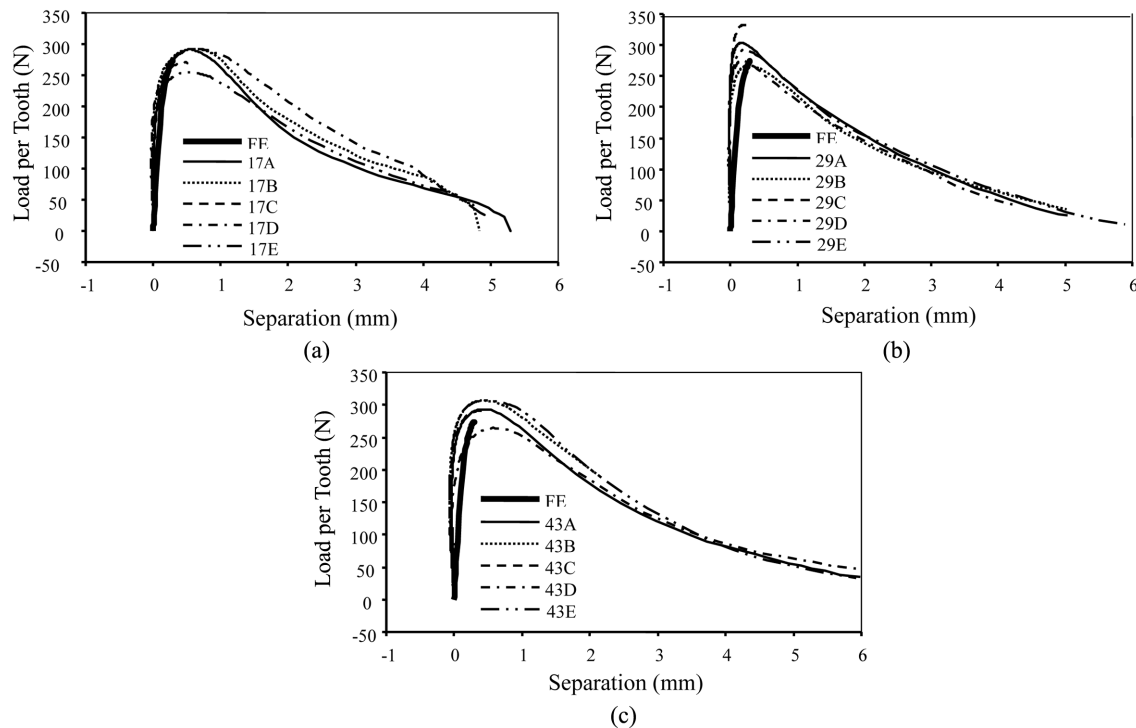


Fig. 8 Comparison of FE predicted joint separation with test results: (a) in direction, (b) against direction, (c) full nail plate

6. Parametric study and optimisation

6.1 Effect of tooth length

Using ‘damaged’ timber material properties determined and other properties as described for the base case (Zhou 2005), the two-tooth model was used to investigate the effect of tooth length on joint performance. In the preliminary study (Zhou 2005), it was shown that the effective tooth length of 6.5 mm lay at the theoretical boundary for joint failure to change from Mode 2 to Mode 3 under Johansen’s theory (Johansen 1949). Reductions to tooth lengths were considered to examine the effect of the stockiness taking towards Mode 1 failure. An arbitrary lower limit of 4.5 mm tooth length was assumed since it was envisaged shorter teeth would have significantly reduced out-of-plane (of base plate) holding capacity. Two cases of slender teeth were considered. A maximum tooth length of 12 mm was considered since, beyond that, it was envisaged that the slenderness would make it difficult for the plates to be pressed in during fabrication, unless a heavier gauge of plate was used. The effects of varying the tooth length are shown in Fig. 9. The load carrying capacity, as expected, falls with decreasing tooth length. It can also be seen that the numerical model handled the shortest tooth length and the slender teeth better than medium length teeth. This may be due to the contact problem whereby the meshes are better matched for these cases.

The Mises stress distribution in the long teeth models is shown in Fig. 10. The stress distribution in the base plate is consistent with moment loading at the tooth root interface as postulated in Fig.

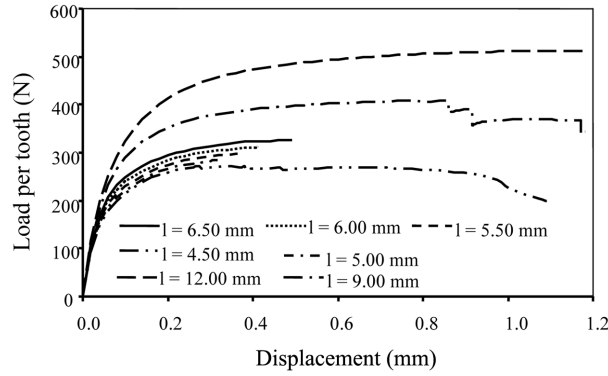


Fig. 9 Modelled load-slip curves for various tooth lengths

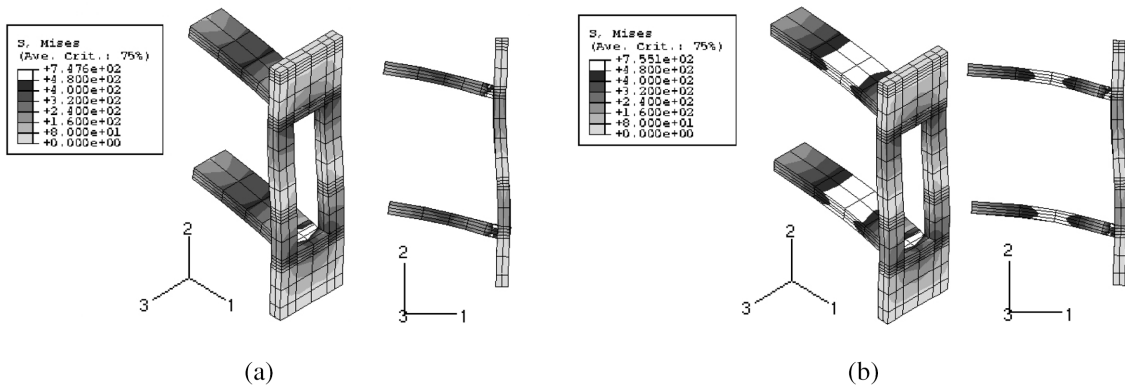


Fig. 10 Failure modes: (a) for 9 mm long teeth, (b) 12 mm long teeth

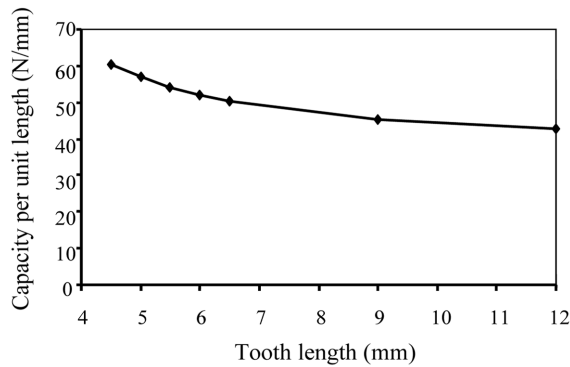


Fig. 11 Effect of tooth length on capacity per unit length

6. The double-curvature buckling shape is also evident in the deflected shape of the models. The white portions in the contours indicate the regions where the Von Mises stresses have exceeded the yield strength of the steel tooth. It is clear that with increase in tooth length failure in the joints changes from Mode 2 to Mode 3 under Johansen’s theory (Johansen 1949). Whereas yielding in shorter teeth occurs in the tooth root area first, longer teeth tend to yield first on the length.

The effect of varying tooth length is assessed in terms of the capacity per unit length of tooth as

shown in Fig. 11. It is clear that the tooth capacity per tooth falls with tooth length. This is in agreement with Johansen's theory of failing joint capacity with increasing mode of failure. Also, the effect of increasing slenderness on reducing developed effective embedding strength is evident. This is in agreement with Trayer's (Trayer 1932) findings of falling embedding strengths with increasing slenderness of fasteners. There are other factors such as resistance to pressing in and pull-out, the cost of punching many small slots and the practicability of tooling the desired slot size having a major influence on the optimum tooth length. Therefore, without further study of the associated factors, it is not possible to arrive at a suggestion of optimum tooth length.

6.2 Effect of tooth width

The original overall dimensions of the nail plate and the centre-to-centre spacing of the tooth rows were maintained for the parametric study. Only the nail plate tooth widths were varied. There are five cases considered, i.e., 3.00 (Original nail plate), 3.25, 3.50, 3.75 and 4.00 mm.

The load-slip curves for the five joint cases modelled are shown in Fig. 12. Base plate buckling shows up as minor plateaus before the maximum load in the curves for the 3.75 mm and 4 mm wide tooth cases.

It is clear that with increase of the tooth width, its load carrying capacity and the initial stiffness are also increased, but its ductility decreased. With increasing the tooth width by 33%, the corresponding load carrying capacity increases by 18%. However, improvement of the initial stiffness is not significant.

Fig. 13 shows the typical joint deformation in the tooth zones of the one-eighth models. The timber beneath the teeth is crushed and gaps open up on the opposite sides. Nail plate withdrawal from the wood can also be seen from the gaps at the tooth ends. There are large separations between the root of the tooth and the timber, which play an important role for tooth pulling-out with further development of the separations. There are also small location separations between the base plate and the timber. It is worth pointing out that the contact between the tooth and the timber is not symmetrical, which is a major contribution factor to the deformation pattern of the base plate. Therefore, if the local deflections on the base plate can be minimised by optimising the tooth layout on it, the critical load to initiate the tooth pull-out can be increased. This should contribute to overall improvement of the joint load carrying capacity.

In this parametric study, the main focus was on the nail plate behaviour. For each joint failure, the

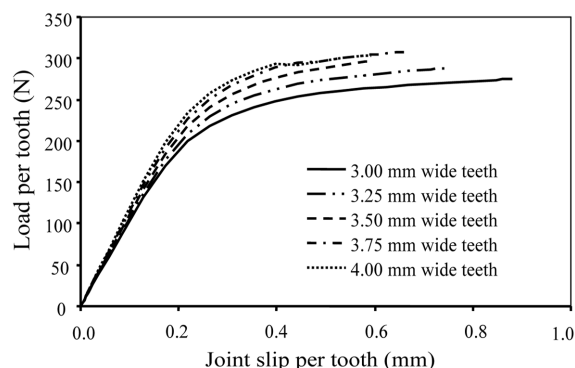


Fig. 12 Load-slip curves for nail plate optimisation models

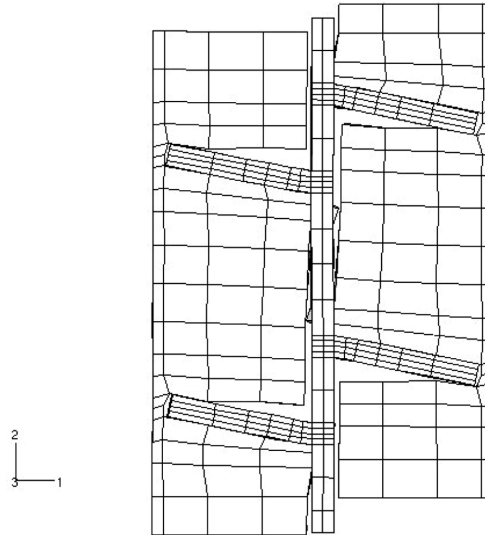


Fig. 13 Joint deformation in the connected zone

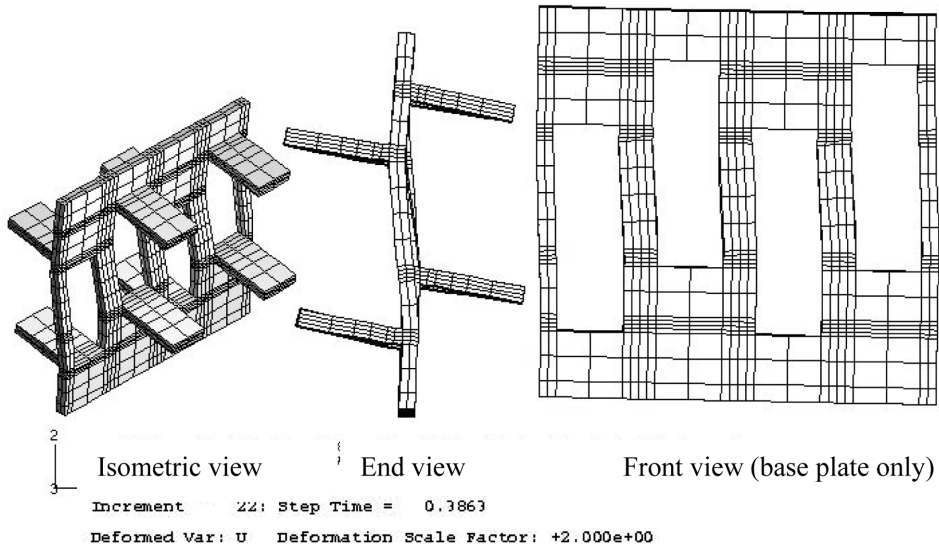


Fig. 14 Deformed shape of nail plate at maximum load – 4 mm wide teeth

state of the nail plate module was examined. As an example, the deformed shape of the nail plate for the upper bound tooth width of 4 mm is shown in Fig. 14.

A deformation scale factor of 2 was used to improve the visualisation of the deformed shapes. Double-curvature buckling of the base plate in the 1-2 plane caused by force-couple moments became very clear due to a large tooth width. However, tooth rotations about the root were minimal.

6.3 Nail plate stress states at ultimate

The stress states at maximum load for the modelled cases are shown in Fig. 15 for two extreme

tooth widths. A contouring upper limit of 336 N/mm^2 was set in the plots in order to track the spread of plasticity in the base plate. The plasticized zones are shown in white.

The stress contours presented are consistent with out-of-plane moments being the major force acting on the base plate. This is in agreement with the supposition illustrated in Fig. 6, which was used to make decisions on where to apply constraints to the base plate to allow parametric studies to be conducted using the two-tooth joint model. Yielding in the base plate is initiated at the tooth root interface where plastic moments are developed as part of the fastener load transfer mechanism. As the base plate columns in between the slots get narrower with increasing tooth widths, the yielding spreads further along the plate length. With the narrower base plate columns, the stress contours also show the increasing influence of the shear buckling induced by eccentric load shearing of the teeth. Throughout the cases analysed, there is very little evidence of significant axial interaction in the plate direction. This implies that similar contours would have been obtained if the direction of load had been reversed. The stress contours presented here support the assumption made at the experimental design stage that the anticipated double-sided nail plate action would have yielded nearly the same joint behaviour under either compression or tension specimen loading.

It is interesting to see that for a given plate thickness, with increasing the tooth width the base plate deflects accordingly following the tooth pattern due to increasing anchorage strength between the tooth and the timber contributed by a larger contact area. When the tooth width is 3.0 mm the base plate deflection is small. However, when such width is 4.0 mm the base plate deflection becomes significant.

6.4 Tooth capacity optimisation

The joint capacities per tooth determined by FE modelling are shown in Fig. 16. The capacities shown were determined from the load-slip data using the 5% of dowel diameter offset method and obtaining the maximum load attained in each model.

The gain in tooth capacity per increment in tooth width is shown in Fig. 17. The 5% offset method was introduced since the load-slip curves showed no definite peak. Use of this method

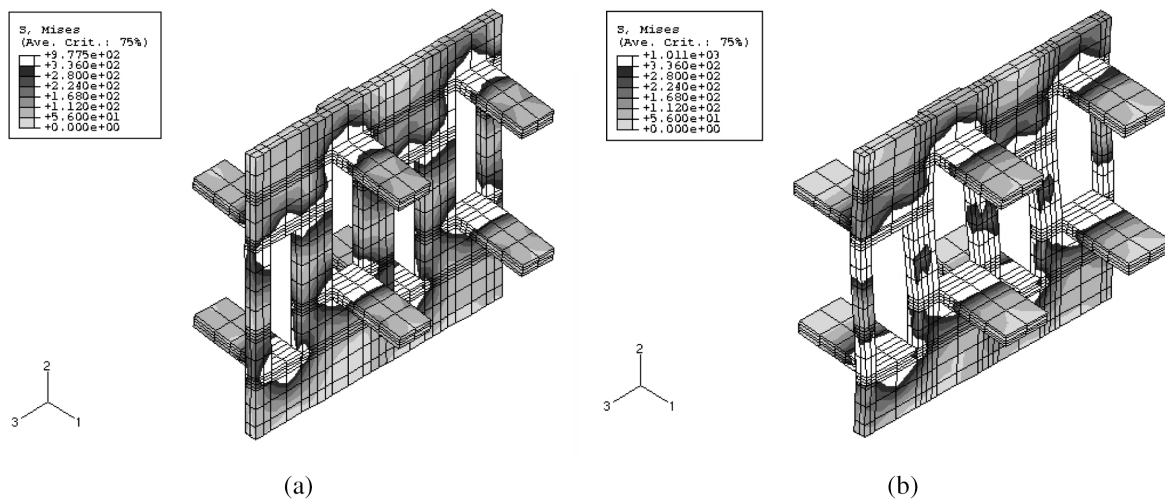


Fig. 15 Mises stress contours for nail plate at maximum load: (a) 3 mm tooth width, (b) 4 mm tooth width

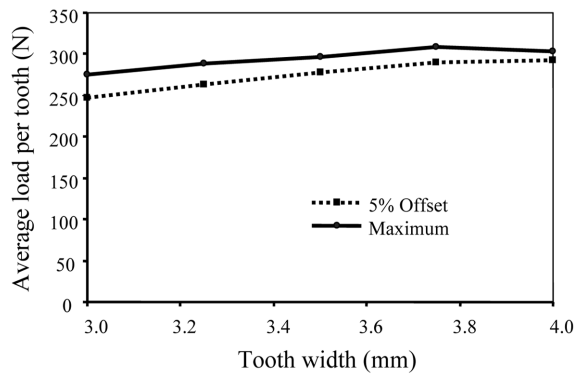


Fig. 16 FE modelled joint capacities per tooth

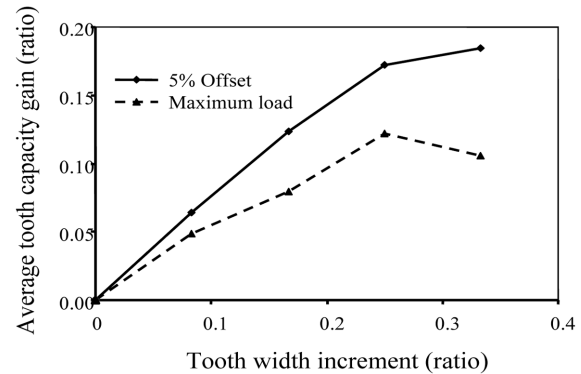


Fig. 17 Normalised tooth width increment to normalised capacity gain

shows that, for the cases modelled, the tooth capacities always increased with tooth width. The maximum load method, however, shows that the tooth capacity peaked at 3.75 mm tooth width. This is a better reflection of the modelled joint performance since it can be seen from Fig. 12 that the 4 mm wide tooth curve plotted just below that for the 3.75 mm wide tooth curve after the base plate buckling. The optimum tooth width can therefore be assumed to lie between 3.75 mm and 4 mm.

7. Discussion on nail plate behaviour towards optimisation

From the deformed shape of the original nail plate configuration, both the tooth and the base plate were stocky, as expected. As the tooth width increased, the tooth itself became stockier, thereby undergoing less rotation, and the base plate columns in between the punched holes became slenderer, thereby undergoing buckling under bending moment and shear loading. Fig. 15 even suggests that, for the slenderest cases, the plate also undergoes twist out of the model 2-3 plane. As seen in the stress contour plots (see Fig. 15), the plasticized region spreads wider from the tooth roots with increasing tooth widths. This complex interaction of failure modes aggravates the non-linear response of the nail plate joint problem. With the contact and wood non-linearity added, it is not surprising that the solutions diverged after the maximum load was attained in each model joint.

From Fig. 17, it is clear that the magnitude of tooth capacity gain is less than that of the tooth width increment, on the basis of individual ratios. This may be attributable to the interaction of base plate column and tooth root capacities, with column capacity decreasing for increasing tooth root capacity. Using the maximum load method, the largest capacity gain achieved was about 12% for a 25% tooth width increment.

The exact tooth width at which maximum capacity is attained could have been established by iterating tooth widths between 3.75 mm and 4 mm and remodelling the joints. Such an exercise, however, would serve little purpose as the potential gain in capacity is likely to be minimal. Also, it must be realised that smaller base plate column widths are likely to lead to significant base plate distortion problems during joint pressing. Therefore, the case for optimisation of the prescribed double-sided punched metal plate is concluded here.

8. Conclusions

Finite element simulations have been developed to successfully model structural behaviour of punched steel plate fasteners. Modelling of contact conditions in the joint is the most essential feature to obtain reasonable simulations. In addition, metal plasticity for steel plate and embedding performance of the tooth against the timber played important roles in development of single-tooth, two-tooth and eight-tooth models. Using validated models, parametric studies were undertaken to investigate effects of the tooth length and the tooth width on joint load carrying capacity. Joint separation and base plate deformation modes have also been modelled. Based on the parametric studies, for the given base plate thickness the optimum tooth width seems lying between 3.75 mm and 4 mm in terms of the tooth capacity. However, without further study of the associated factors such as resistance to pressing in and pull-out, the cost of punching many small slots and the practicability of tooling the desired slot size, it is not possible to arrive at a suggestion of optimum tooth length. More work is required to be undertaken to develop comprehensive full-joint models to address the above factors, also other parameters such as the base plate thickness and the tooth pattern.

References

- Adjanohoun, G., Rouger, F. and Talbi, N. (1999), "Semi-rigid behaviour of a stamped metal teeth connector under static loads", In *COST C1, Semi-rigid Timber Joints - Structural Behaviour, Modelling and New Technologies*, Final Report of Working Group "Timber Joints", ed. Haller, P. Dresden.
- Bodig, J. and Jayne, B.A. (1982), *Mechanics of Wood and Wood Composites*, London: Van Nostrand Reinhold.
- Chen, W.F. and Han, D.J. (1988), *Plasticity for Structural Engineers*, Springer-Verlag Inc., News York.
- Cramer, S.M. (1990), "Theoretical consideration of metal plate connected wood splice joints", *J. Struct. Eng.*, ASCE, **116**(12), 3458-3474.
- Drucker, D.C. (1988), "Conventional and unconventional plastic response and representation", *Appl. Mech. Rev.*, **41**, 151-167.
- Forest Products Laboratory (1999), *Wood Handbook - Wood as an Engineering Material*, Gen. Tech. Rep. FPL-GTR-113. Madison, WI. U.S. Department of Agriculture.
- Foschi, R.O. (1977), "Analysis of wood diaphragms and truss, Part II: Truss-plate connections", *Can. J. Civil Eng.*, **4**(3), 353-362.
- Foschi, R.O. (1979), "Truss plate modelling in the analysis of trusses", *Proc. Metal Plate Wood Truss Conf.*, Madison WI. Forest Products Research Society, 88-97.
- Guan, Z.W. and Rodd, P.D. (2000), "Hollow steel dowels – A new application for semi-rigid timber connections", *Eng. Struct.*, **23**(1), 110-119.
- Guan, Z.W. and Rodd, P.D. (2001), "DVW – A local reinforcement in timber connections", *J. Struct. Eng.*, ASCE, **127**(8), 894-900.
- Guan Z.W. and Rodd, P.D. (2003), "Numerical modelling of timber connections locally reinforced by DVW discs", *Struct. Eng. Mech.*, **16**(4), 391-404.
- Guan, Z.W. and Rodd, P.D. (2005) "Study of glulam beams prestressed with pultruded GRP", *Comput. Struct.*, **83**, 2476-2487.
- Hibbitt, Karlsson & Sorensen, Inc. (2002), *ABAQUS/Standard User's Manual*, Version 6.3, Pawtucket, RI, USA.
- Hill, R. (1948), *A Theory of the Yielding and Plastic Flow of Anisotropic Materials*, Proceedings of the Royal Society, 189-297.
- Johansen, K.W. (1949), *Theory of Timber Connections*, International Association of Bridge and Structural Engineering, Publication No. 9:249-262. Bern.
- Malinowski, C. (1985), "Untersuchung mit Nagelübeln als Holzverbindungsmittel - Teil 1: Versuche zur

- Ermittlung einer günstigen Formgebung und geeigneter Anwendungsbereiche”, *bauen mit holz*, 1/85 (Translated July 2004 by Jochen Riederer as: “Research about nail dowels as timber fastener - Part 1: Experiments to examine a promising design and suitable fields of application”.
- Nayak, G.C. and Zienkiewicz, O.C. (1972), “Elasto-plastic stress analysis: Generalization for various constitutive relations including strain softening”, *Int. J. Numer. Meth. Eng.*, **5**, 113-135.
- Pattern-Mallory, M., Cramer, S.M., Smith, F.W. and Pellicane, P.J. (1997), “Nonlinear material model for analysis of bolted wood connections”, *J. Struct. Eng.*, ASCE, **123**(8), 1063-1070.
- Rahman, M.U., Rowlands, R.E., Cook, R.D. and Wilkinson, T.L. (1984), “An iterative procedure for finite-element stress analysis of frictional contact problems”, *Comput. Struct.*, **18**, 947-954.
- Reiterer, A. and Stanzl-Tschegg, S.E. (2001), “Compressive behaviour of softwood under uniaxial loading at different orientations to the grain”, *Mech. Mater.*, **33**, 705-715.
- Šilih, S., Premrov, M. and Kravanja, S. (2005), “Optimum design of plane timber trusses considering joint flexibility”, *Eng. Struct.*, **27**(1), 145-154.
- Trayer, G.W. (1932), *The Bearing Strength of Wood Under Bolts*, US Department of Agriculture Technical Bulletin No. 332.
- Zhou, T. (2005), *Towards Optimisation of a Double-sided Punched Metal Nail Plate Connector*, Ph.D. thesis, University of Brighton.
- Zhu, E.C. (2003), *Modelling the Structural behaviour of OSB Webbed Timber I-beams*, PhD thesis, University of Brighton.
- Zhu, E.C., Guan, Z.W., Rodd, P.D. and Pope, D.J. (2005), “Parametric studies of the interaction between openings in OSB webbed timber I-beams”, *Adv. Eng. Software*, **36**, 797-805.
- Wolfe, R.W., Stahl, D.C. and Cramer, S.M. (1996), *Experimental Assessment of Wood Trusses with Square-end Webs*, *Research Paper FPL-RP-544*, Forest Products Laboratory, USDA, Madison WI, USA.

Notation

- $\{b\}$: vector related to Hill’s yield function
 $[C]_{orth}$: orthotropic elastic compliance matrix
 $[D]_{ep}$: elasto-plastic matrix
 E_2, E_L : Young’s modulus for the longitudinal direction
 E_3, E_R : Young’s modulus for the radial direction
 E_1, E_T : Young’s modulus for the tangential direction
 $f(\sigma_{ij})$: yield function
 G_{23}, G_{LR} : shear modulus for the radial- longitudinal plane
 G_{31}, G_{RT} : shear modulus for the radial-tangential plane
 G_{12}, G_{TL} : shear modulus for the tangential-longitudinal plane
 p : contact pressure acting normal to the contact surface
 R_{ij} : yield ratio
 $\{\epsilon\}$: strain tensor
 $\{d\epsilon_{ij}\}$: incremental total strain tensor
 $\{d\epsilon_{ij}\}_{el}$: incremental elastic strain tensor
 $\{d\epsilon_{ij}\}_{pl}$: incremental plastic strain tensor
 $d\lambda$: plastic multiplier
 μ : coefficient of friction
 ν_{TL} : Poisson’s ratio for the tangential-longitudinal plane ($=\nu_{12}$)
 ν_{TR} : Poisson’s ratio for the tangential-radial plane ($=\nu_{13}$)
 ν_{LR} : Poisson’s ratio for the longitudinal-radial plane ($=\nu_{23}$)
 ν_{LT} : Poisson’s ratio for the longitudinal-tangential plane ($=\nu_{21}$)
 ν_{RL} : Poisson’s ratio for the radial-longitudinal plane ($=\nu_{32}$)
 ν_{RT} : Poisson’s ratio for the radial- tangential plane ($=\nu_{31}$)
 $\{\sigma\}$: stress tensor

- $\bar{\sigma}_{ij}$: yield level for stress component
- σ^o : reference timber yield strength
- τ^o : the nominal yield shear strength for Hill's yield theory
- τ_R : limiting frictional shear stress
- F_{ii}, N_{ij} : constants in Hill potential function